Organic Process Research & Development

ARTICLE

pubs.acs.org/OPRD

Optimization of a Crystallization by Online FBRM Analysis of Needle-Shaped Crystals

Tom Leyssens,*[,†] Carine Baudry,[‡] and Maria Luisa Escudero Hernandez[‡]

[†] Université Catholique de Louvain, Place Louis Pasteur 1, 1348 Louvain-la-Neuve, Belgium

[‡] UCB Pharma, Chemin du Foriest, 1420 Braine l'Alleud, Belgium

Supporting Information

ABSTRACT: In this contribution, the FBRM probe is used to investigate a crystallization of needle-shaped particles to develop a crystallization that can deliver product within the required quality attributes. The crystallization under study is that of CDP323-2, a small-molecule prodrug antagonist. As the particles do not show a spherical shape habit, particular care has to be taken when interpreting FBRM chord length distributions. Case-specific chord length distribution (CLD) properties are defined for needle-shaped particles to study primary and secondary nucleation, as well as crystal growth and breakage during the crystallization. Results show the crystallization of CDP323-2 to be characterized by a very rapid longitudinal growth after nucleation. During the initial stages of cooling, crystal growth kinetics dominate secondary nucleation, but this tendency is reversed for the lower temperatures of the cooling profile. The FBRM is shown to be a powerful tool that can bring valuable insight, even for the crystallization of nonspherically shaped particles.

1. INTRODUCTION

Crystallization is often the final step in the total production of an active pharmaceutical ingredient (API). It allows the purification and isolation of the final product in a single step. The crystallization stage in a production process is extremely important and must guarantee the quality of the product[1] by assuring high purity, the desired particle size distribution (PSD), and a crystalline morphology.[2,3] Although of manifest importance, often little effort is placed into the development of a crystallization process, and hence, it is often poorly controlled.[4] Good control requires a knowledge of the cause and effect of the influential factors of, amongst others, temperature,[5] concentration,[6] impurity level, stirring speed and type, and antisolvent addition rate.[7] Over recent years, numerous advances have been made in the area of crystallization. The development of powerful online analytical sensors has allowed a better understanding and control of the process.[8−10] In addition to the increased amount of data gained from real-time measurements, they have the advantage of avoiding the effect of external perturbations in their measurements, as can be typically seen when applying classical off-line sampling techniques. The process analytical technology (PAT) guidance announced by the U.S. Food and Drug Administration, encourages the use of such techniques, explaining why these tools are becoming an integral part of many API production facilities. The use of PAT[11−14] allows an online measurement and direct control of the critical process parameters[15,16] and therefore a greater warranty of the quality attributes of the product. It is without doubt one of the most appropriate tools used when implementing quality by design in manufacturing processes.[17]

The Lasentec focused beam reflectance measurement (FBRM)[18,19] can be used to understand and control different aspects of a crystallization procedure. The FBRM probe measures a chord length distribution (CLD),[20] which is a function of the number, size, and shape of the particles in suspension. Relating chord length distributions to particle size distributions is, nevertheless, not straightforward and requires extensive modeling.[21,28]

Nevertheless, variations in the properties of the CLD over time can help to characterize physical mechanisms such as primary and secondary nucleation,[22−24] crystal growth,[25,26] ripening, attrition, crystal breakage, aggregation, and agglomeration. However, definition and interpretation of CLD properties, and their link to physical mechanism, has not been thoroughly investigated,[27,28] especially when dealing with particles of nonspherical shape,[29−32] even though these tools are more often used to investigate crystallizations of such particles.[33] The key objective of this article is to show how CLD properties can be defined for needle-shaped particles, and how their variation over time can be linked to different physical mechanisms of crystallization. The ultimate goal is the delivery of product within the required quality attributes in a reproducible manner through the optimization of the different influential parameters.

The crystallization under study is that of the final drug substance CDP323-2; a small-molecule prodrug antagonist for the treatment of multiple sclerosis. CDP323-2 is the hydrated sulfate salt obtained from crystallization of a CDP323 in $EtOH/H_2O/H_2SO_4$ solution (Figure 1), to yield particles with a distinct needle-shaped crystal habit. Although different forms of the CDP323 hydrated sulfate salt exist, under the defined operating conditions, CDP323-2 is the only form observed. All of CDP323 salt forms show needle-shaped crystal habits. [The solid-state properties of the different salt forms, as well as their

Received: November 29, 2010
Published: March 03, 2011

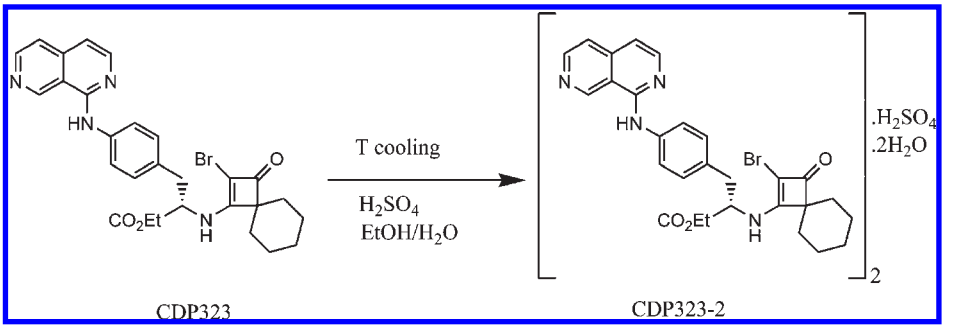

Figure 1. Crystallization of needle-shaped CDP323-2 from a CDP323 in $EtOH/H_2O/H_2SO_4$ solution.

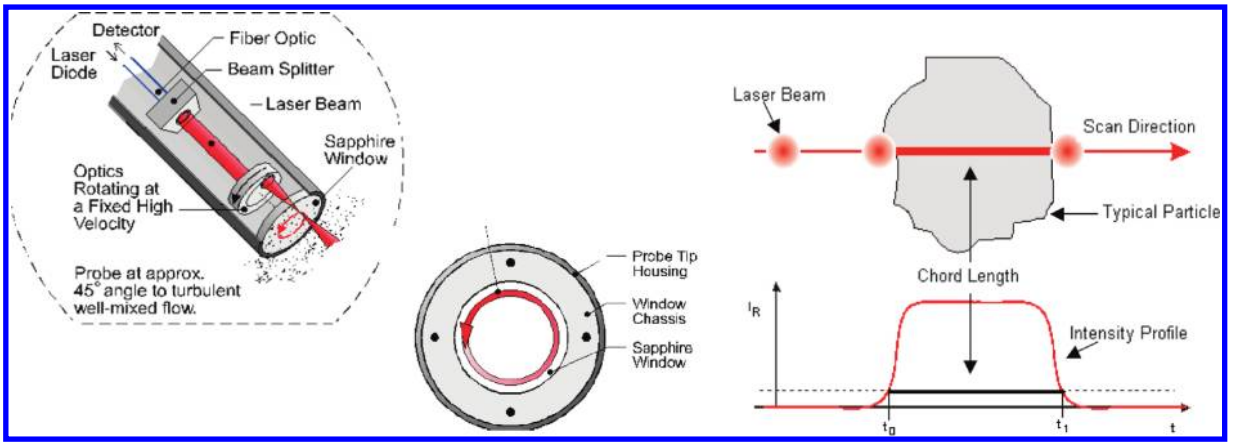

Figure 2. FBRM operating principle: probe tip sends out a circular laser beam, and the intensity of reflected light can be translated into a particle chord length.[34].

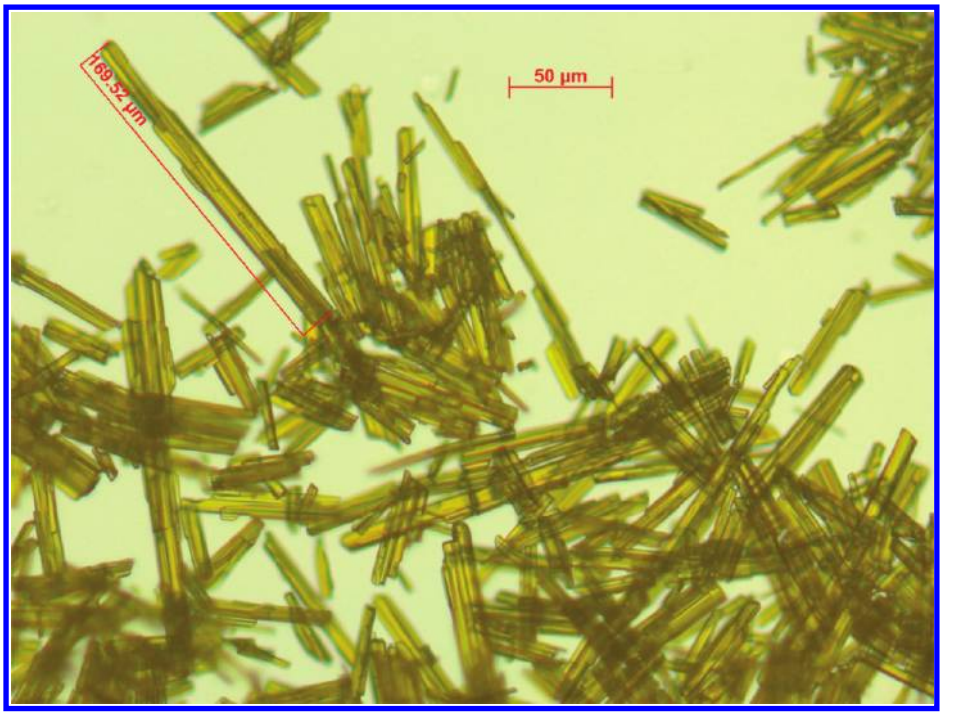

Figure 3. Optical microscopy image of CPD323-2 crystals, exhibiting a needle-shaped habit.

stability under given conditions, will be treated in a future contribution.[38]] For development purposes, an optimized cooling profile was developed to reduce process time while maintaining relatively broad needle-shaped crystals.

dx.doi.org/10.1021/op100314g |*Org. Process Res. Dev.* 2011, 15, 413–426

2. FOCUSED BEAM REFLECTANCE MEASUREMENT (FBRM)

The FBRM (Figure 2) uses a focused beam of monochromatic laser light rotating at a constant speed of 2 m s^{-1}. The focal point is maintained at a fixed plane of −20 μm, just inside the sapphire window for the duration of the scan, thereby ensuring maximum sensitivity to particle changes even at high solid loading per unit volume. As particles pass in front of the probe window, light is backscattered from particles on or close to the sapphire window. The duration of the backscatter is measured and related to a particle chord length as shown in Figure 2. The chord length hence measures the distance of a straight line between any two points on the edge of a crystal. Typically, many thousands of chords are measured per second, providing a precise measurement that is sensitive to the change in the dimension and number of particles. Chord lengths are categorized according to length, counted, and collected in a number-based chord length histogram from which the chord length distribution can be extracted.

Crystallized CDP323-2 shows a needle-shaped habit as shown in Figure 3.

When interpreting FBRM chord length distributions, a strong increase in the number of small chord lengths is often associated with an increase in the number of small particles such as those derived from primary or secondary nucleation, whereas an increase in the number of large chord lengths is attributed to crystal growth or agglomeration. When dealing with spherical crystals, this approach is straightforward. However, a more sophisticated interpretation is required when the particles are nonspherical. The lack of a spherical shape habit requires caution when interpreting variations in chord length distributions during crystallizations of these compounds.[29−31] Figure 4 graphically shows that an increase in number of small chord lengths does not necessarily imply secondary nucleation; But can also be indicative of crystal growth. An increase in needle length, will indeed lead to an increase in small chord lengths (red lines in Figure 4) counted over time, as the needle width has a higher probability of being measured/intersected by the scanning laser in comparison to the needle length.

Figure 4. Needle-shaped crystals, showing chord lengths of different sizes.

In the following section, specific CLD properties are defined in order to study primary and secondary nucleation, crystal growth and breakage during the crystallization of needle-shaped particles. The different stages occurring during the crystallization can be identified and studied using combinations of these well-defined statistical CLD properties.

3. STATISTICAL CHORD LENGTH DISTRIBUTION (CLD) PROPERTIES FOR NEEDLE-SHAPED PARTICLES

As mentioned above, to obtain a distribution, chord lengths are categorized according to their length. Different types of classification exist, depending on how the total range (0−1024 μm) is divided. As shown in Figure 4, variations in small chord length statistics will be important to describe crystallizations of needle-shaped particles. High resolution at the small-particle side of the CLD is therefore important, which is achieved using logarithmic grouping of measured chord lengths. Contrary to linear grouping, in logarithmic grouping each channel width is progressively wider than the preceding channel width, and the distance between channel midpoints is proportionate to their logarithms. This provides high resolution on the small-particle side of the distribution, while at the same time providing significantly lower resolution on the large particle side. In this specific study chord lengths between 1 and 1000 μm are distributed over

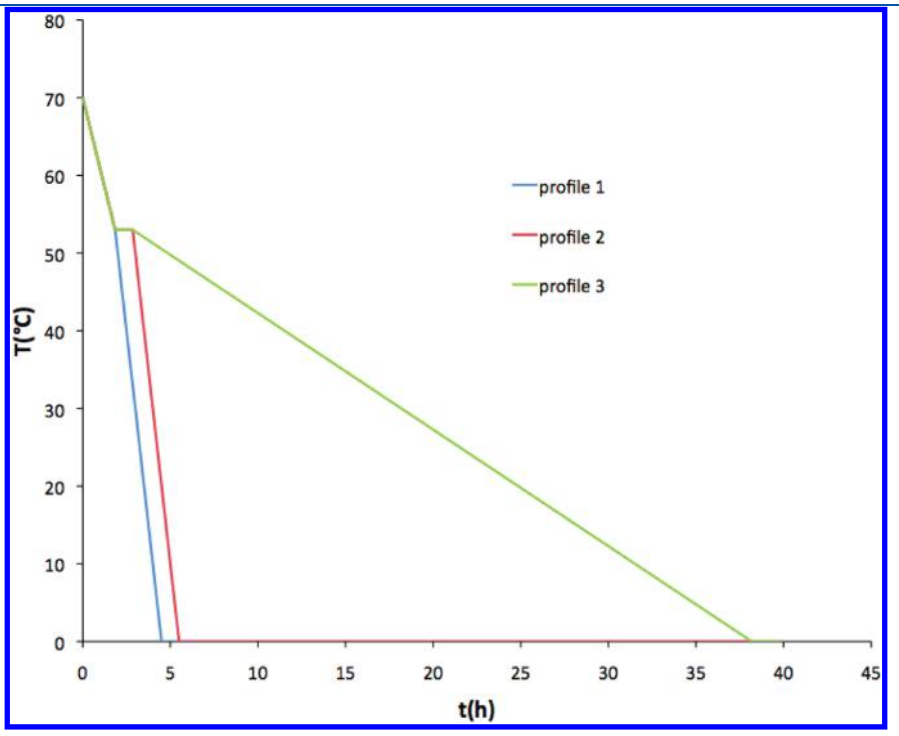

Figure 5. Cooling profiles used throughout this work.

dx.doi.org/10.1021/op100314g |*Org. Process Res. Dev.* 2011, 15, 413–426

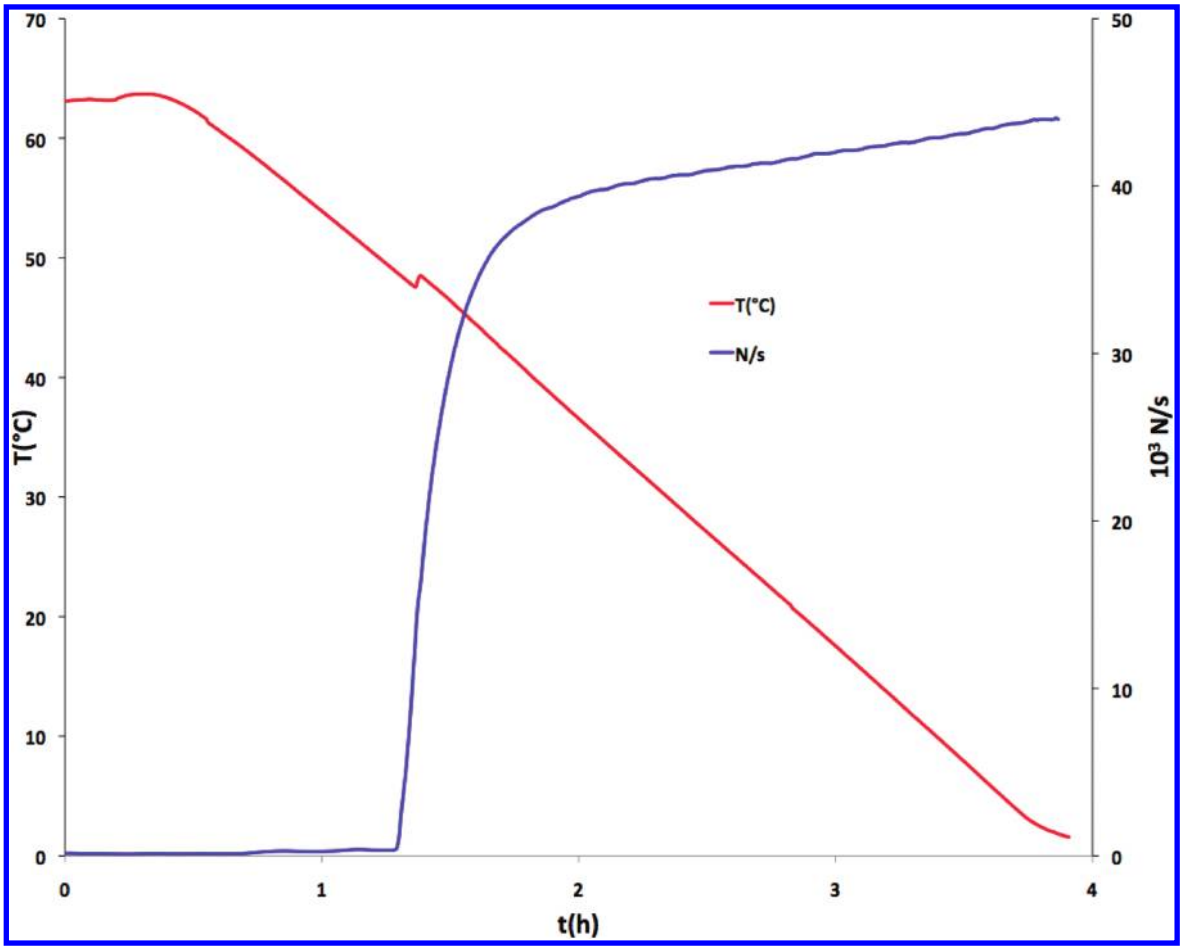

Figure 6. Mass temperature (red curve) and number of nonweighted chord length counts/s (blue curve) over time for a crystallization following cooling profile 1.

90 different channels. The number of counts per channel (n_j) leads to the final CLD.

As for any particle shape (spherical or other) the number of small chord length counts statistically always outweighs the large particle chord length counts. To compensate for this, channel weighting of the total count can be applied in order to emphasize certain regions of the CLD. Channel weighting emphasizes the change in one region of the distribution while deemphasizing the change in another region by applying a channel-specific weight w_j to the number of counts n_j. The weighted-channel counts y_j are obtained via

$$y_j = w_j * n_j \tag{1}$$

For channels $j = 1, 2, ..., N$ ($N = 90$ in this paper). The weights w_j are obtained from the channel midpoints M_j via

$$w_j = \frac{M_j^{\gamma}}{\sum_{j=1}^{N} M_j^{\gamma}} \cdot N \tag{2}$$

Values of $\gamma = 0$ and 2 lead respectively to nonweighted and square-weighted distributions.

Square-weighted CLD or statistical values will therefore place an emphasis on large chord length characteristics, whilst non-weighted values will place a similar emphasis on small chord length characteristics. Statistical values can be taken over different channels, e.g. the mean chord length $\overline{C}$ between 100 and 500 μm is given by

$$\overline{C} = \frac{\sum_{i=a}^{b} y_i M_i}{\sum_{i=a}^{b} y_i} \tag{3}$$

where a denotes the channel starting at 100 μm and b denotes the channel ending at 500 μm. Note that according to the nature of y, the mean can be nonweighted or square-weighted.

To investigate needle-shaped crystals it is important to have an initial idea of their final shape. The optical microscopy image (Figure 3) of a typical batch of CDP323-2 crystals shows needles of about 10 μm in width and of about 100 μm in size. These values help to choose different statistical parameters for the interpretation of the various stages of the crystallization. Below, a list is given of those variables used throughout this work, as well as their physical interpretation. Similar variables can be used to study other needle-shaped crystallizations, as long as boundaries are changed according to the nature of the compound.

- Nonweighted number of chord lengths between 1 and 30 μm counted per second. As the final crystal width is about 10 μm, this variable is dominated by the number of times the laser crosses the needle width. As most of the time the needle will not be crossed exactly perpendicular to

dx.doi.org/10.1021/op100314g |*Org. Process Res. Dev.* 2011, 15, 413–426

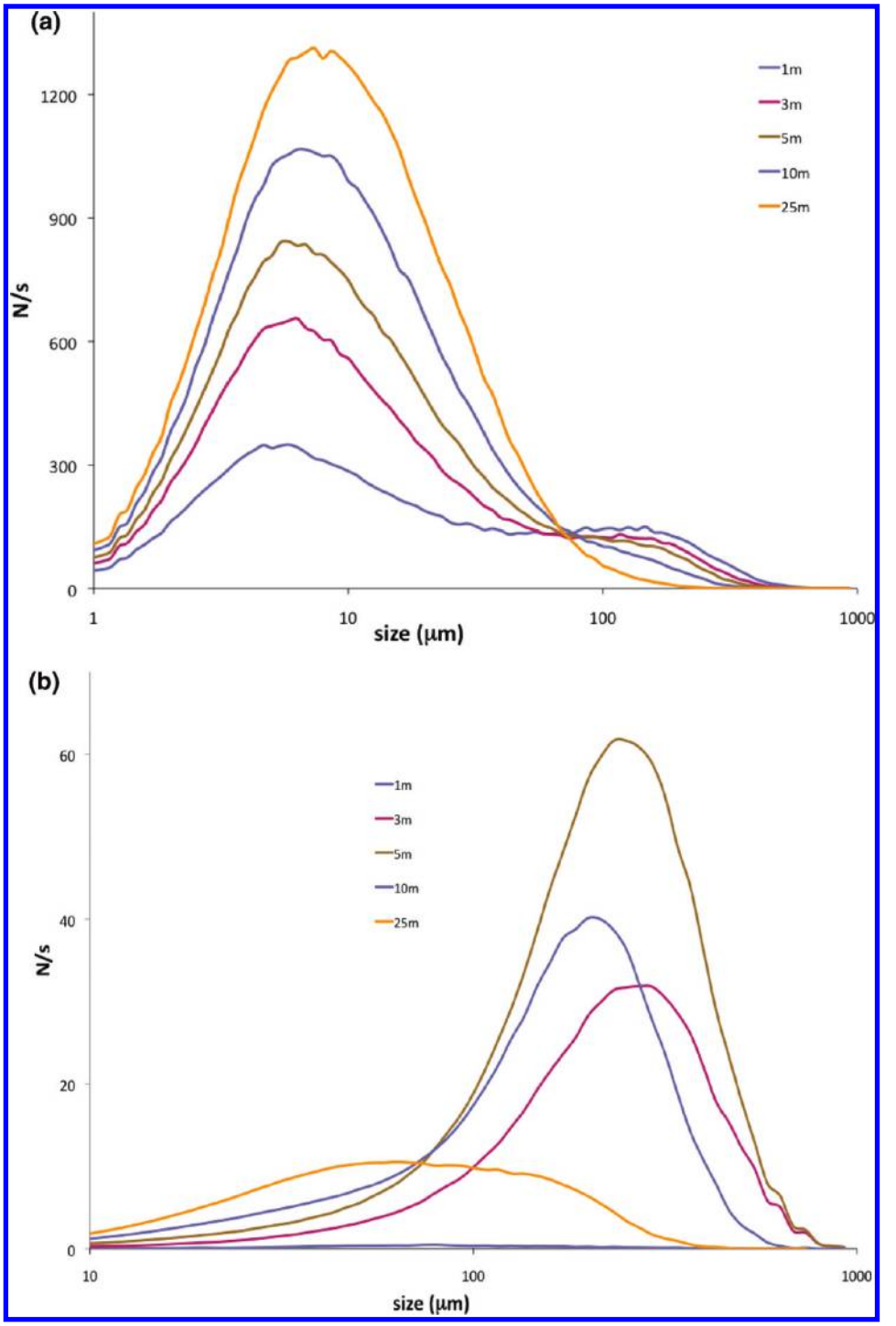

Figure 7. (a) Nonweighted linear chord length distribution over time, after initial crystallization ($t = 0$). (b) Square-weighted chord length distribution over time, after initial crystallization ($t = 0$). [The square-weighted distribution has been time-averaged to achieve smoother curves. Time averaging occurred over 10 measures, and curves were checked to behave similarly to the non-time-averaged curves.] [blue =1 min; brown =3 min; green= 5 min; purple =10 min; yellow =25 min] Log distributions are shown, as these lead to a higher resolution.

the needle length, slightly larger values than 10 μm (up to 30 μm taken in this work) can still be associated with needle width. As the total number of counts corresponds to the number of times the laser crosses the needle, this variable can be related to the total needle length (or total number of needles) in suspension. However, a linear correlation between total counts and concentration is only observed at low solid concentrations for simple particle shapes, i.e. spheres, and the variable should therefore only be used to indicate trends.

- Nonweighted median of chord lengths between 1 and 30 μm counted per second. Following the same reasoning mentioned above, the median of the chord lengths between 1 and 30 μm can be associated with the needle width and

dx.doi.org/10.1021/op100314g |*Org. Process Res. Dev.* 2011, 15, 413–426

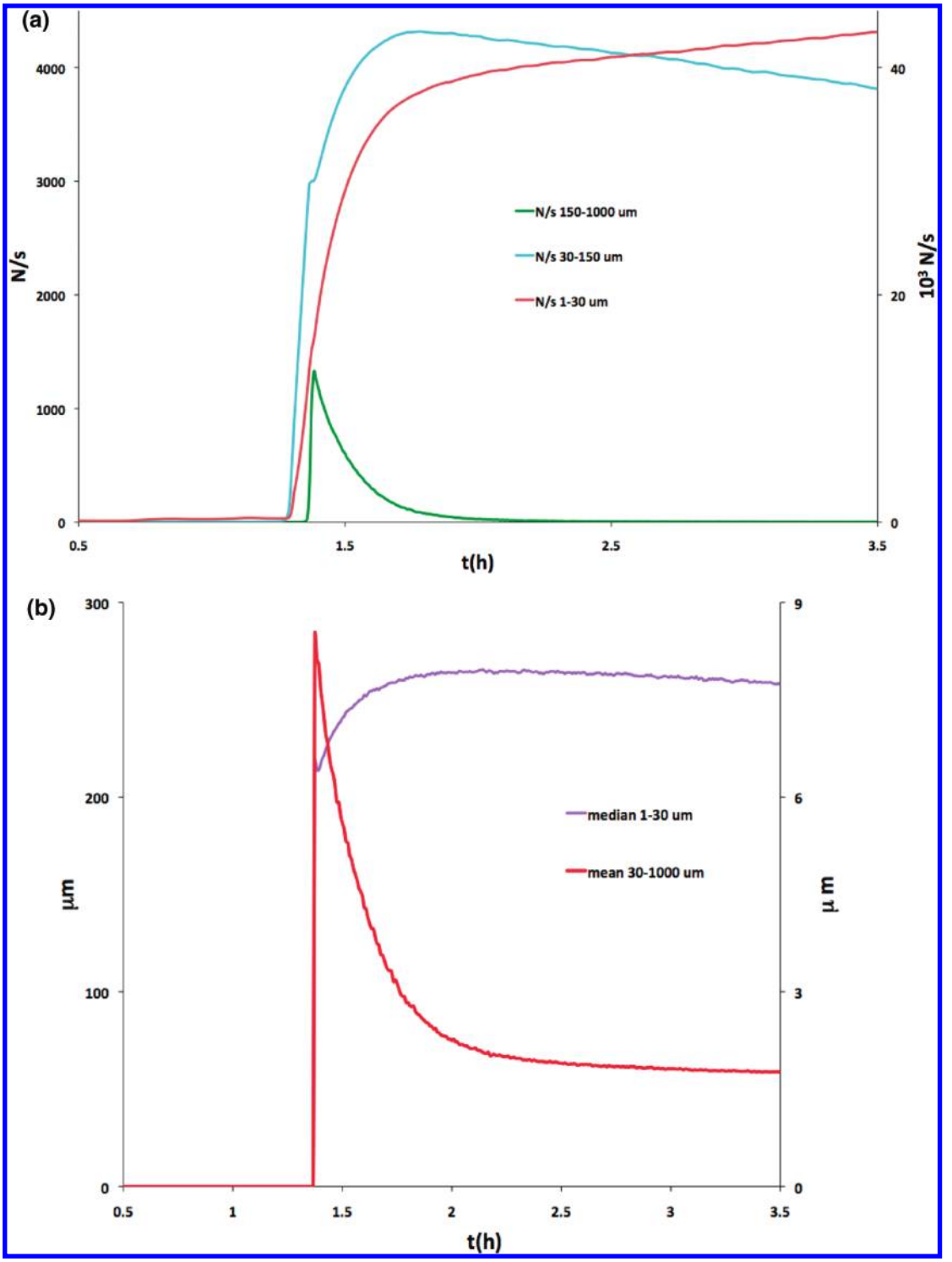

Figure 8. (a) Number of chord lengths counted per second over time between 1 and 30 μm (brown curve/right axis), 30−150 μm (blue curve/left axis), 150−1000 μm (green curve/left axis). (b) Median chord lengths counted per second between 1 and 30 μm (purple curve/right axis), square-weighted mean chord lengths per second between 30 and 1000 μm (red curve/left axis).

more specifically gives an estimation of the average needle width.

- Nonweighted number of chord lengths between 30 and 150 μm counted per second. As the optical microscopy images show a final needle length of about 100 μm, chord lengths measured between 30 and 150 μm are due to the interaction with crystals of average to large length. The total count is indicative of the amount of these crystals.
- Nonweighted number of chord lengths between 150 and 1000 μm counted per second. Chord lengths measured between 150 and 1000 μm in turn are due to the interaction with crystals of very large length. The total

dx.doi.org/10.1021/op100314g |*Org. Process Res. Dev.* 2011, 15, 413–426

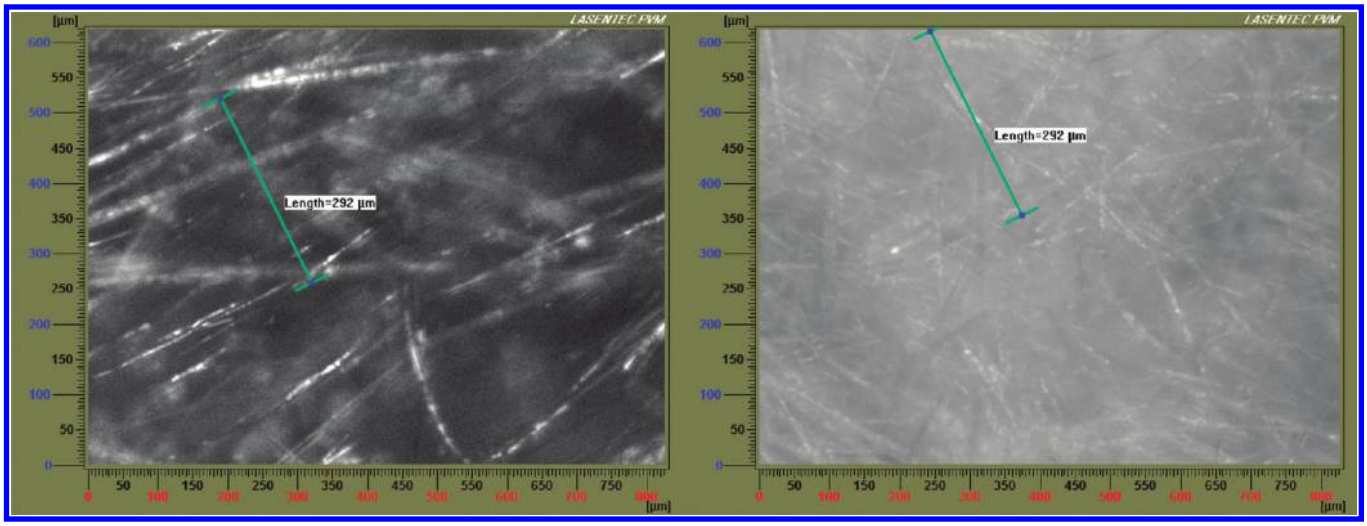

Figure 9. Process video microscope (PVM) images taken during the first 10 min after nucleation (left) and 60 min after nucleation (right).

count can be directly related to the amount of these crystals.

- Square-weighted mean of chord lengths between 150 and 1000 μm counted per second. This mean can be seen as a measure of the average length of the very large needle-shaped crystals.
- Square-weighted mean of chord lengths between 30 and 1000 μm counted per second. This mean can be seen as a measure of the average length of the needle-shaped crystals (measurements smaller than 30 μm are predominately measurements of needle width).

To study the different phases of a crystallization process, the above-mentioned parameters were combined appropriately as shown in the Discussion of the Results. The statistical parameters considered in this report led to a coherent understanding of the crystallization of needle-shaped crystals.

4. EXPERIMENTAL SETUP

For each experiment 100 g of CDP 323 was charged in a 2-L automated reactor equipped with a glass anchor stirrer and temperature probe. The stirring rate was set at 150 rpm. Lasentec FBRM and particle video microscopy (PVM) probes were introduced into the reactor. The latter allows an online collection of video images during the crystallization, which provide additional information to improve process understanding. Added to the suspension were 642 mL of EtOH and 150 mL of H_2O, and the suspension was heated up to 70 °C to ensure complete dissolution. Added over a 15-min time period was 0.5 equiv of H_2SO_4 in 100 mL of H_2O. At this point, the total solvent composition was 72% v/v EtOH, and the final concentration in CDP323-2 was 12.91% w/w with respect to the total weight of the solution. The solubility temperature for this concentration was determined to be 58 °C. [The solubility curve of CDP323-2 in a EtOH/H_2O 70% v/v solvent system is given in the Supporting Information.] Different cooling profiles were then applied depending on the factor studied.

5. DISCUSSION OF THE RESULTS

5.1. Cooling Profiles. The goal of this study was the optimization of the crystallization via online monitoring of the crystal nucleation and growth in order to reduce process time while maintaining relatively broad needle-shaped crystals. Different cooling scenarios were considered to understand the influence of the temperature parameters on the underlying crystallization mechanisms.[35] Figure 5 shows the three different temperature profiles used throughout this work.

Profile 1 (blue curve) consisted of a constant cooling rate of 20 °C/h from 70 to 0 °C followed by an overnight isothermal hold. This allowed the determination of the crystallization temperature and the detection of changes in physicochemical behavior during a continuous cooling profile. Profile 2 was tested in order to compare with a seeded crystallization. Profile 2 consisted of a rapid cooling (20 °C/h) to 53 °C followed by seeding with 0.2% w/w of CDP323-2 with respect to the CDP323 input. The seeds were left to mature for 1 h at the seeding temperature after which a cooling ramp of 20 °C/h was applied to reach the final isolation temperature. The suspension was left stirring overnight at 0 °C. This profile allowed studying the effect of seeding[36] and the physicochemical changes occurring during the isothermal hold at 53 °C. In profile 3 (green), the effect of a slow cooling profile was investigated by repeating the seeded crystallization, but using a cooling ramp of 1.5 °C/h. All three profiles were executed by controlling the jacket temperature.

5.2. Spontaneous Crystallization. The nonseeded experiment shows a spontaneous nucleation at about 48 °C, at which stage a relative supersaturation of 98% was attained. The spontaneous nucleation is characterized by a strong increase in the total number of chord length counts per second, as well as a crystallization exotherm, as seen in Figure 6. This strong increase in total number of counts lasts about 20 min. After this period, the total number of chord length counts still increases but less rapidly. To study the spontaneous nucleation, the first 20-min time period was considered.

Comparing the overall weighted and nonweighted distributions over time (Figure 7), one notices a strong increase in large to very large particles at the onset of crystallization, leading to a bimodal distribution, as shown for the curve obtained after 3 min. The shoulder behavior of the CLD is rarely observed for nonweighted distributions (Figure 7a), as the small chord length counts usually strongly outweigh the number of large particles present. Furthermore, whereas the peak corresponding to the small chord lengths (up to 50 μm) rapidly increases over the

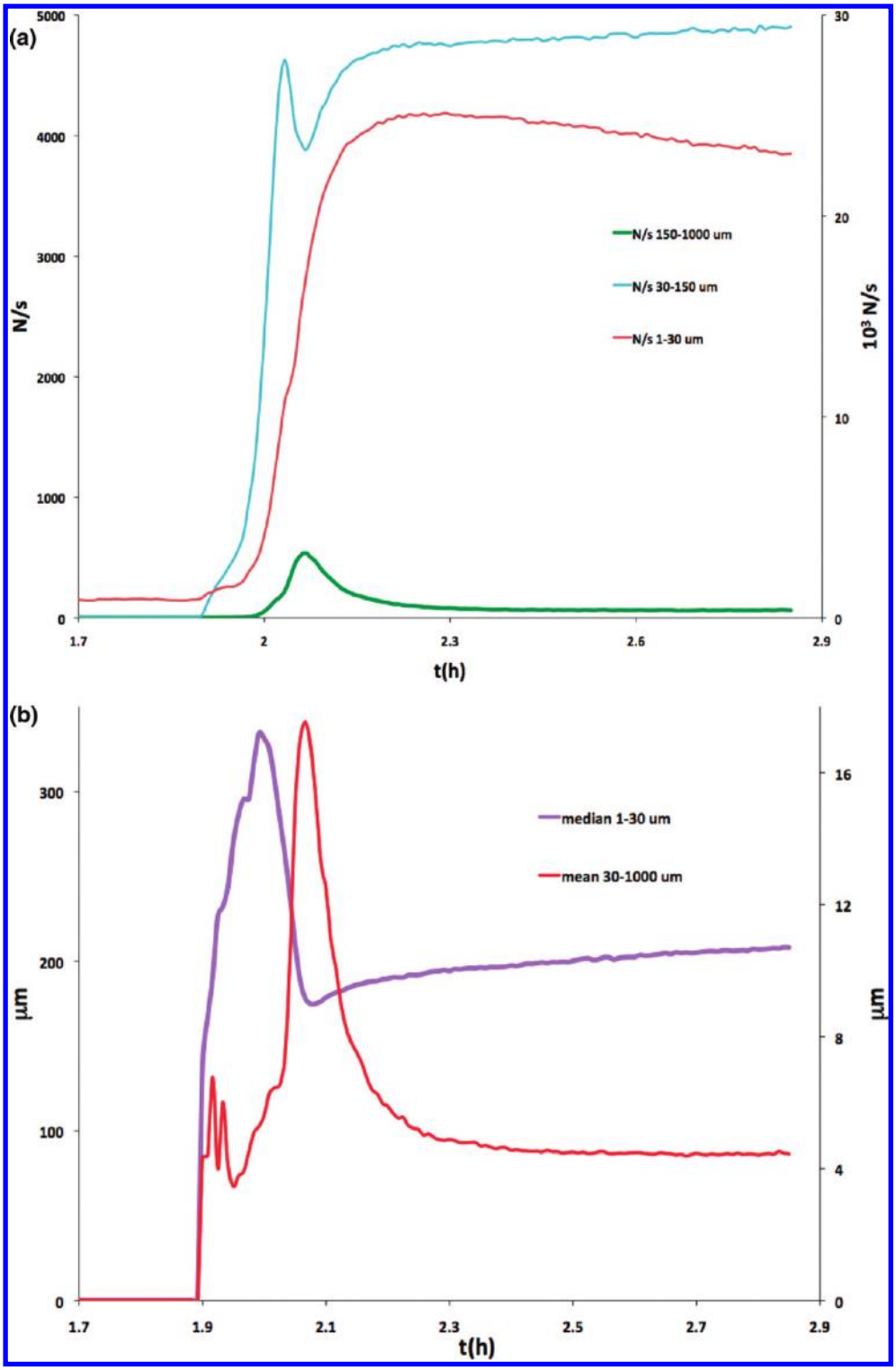

Figure 10. (a) Number of chord lengths counted per second over time between 1 and 30 μm (brown curve/right axis), 30−150 μm (blue curve/left axis), 150−1000 μm (green curve/left axis). (b) Median chord lengths counted per second between 1 and 30 μm (purple curve/right axis), square-weighted mean chord lengths per second between 30 and 1000 μm (red curve/left axis).

entire time span considered, the shoulder increases for the first 3 min but then decreases over the next 20 min leading one to believe that at the onset of crystallization the number of large to very large particles is important. This is confirmed by considering the square-weighted CLD (Figure 7b), characterized by a strong and rapid increase in large particle population during the first 5 min followed by a decrease of the number of large particles during the following 20 min. This behavior is consistent with a primary nucleation of a limited number of needle-shaped crystals that grow at a very fast rate at the onset of crystallization.

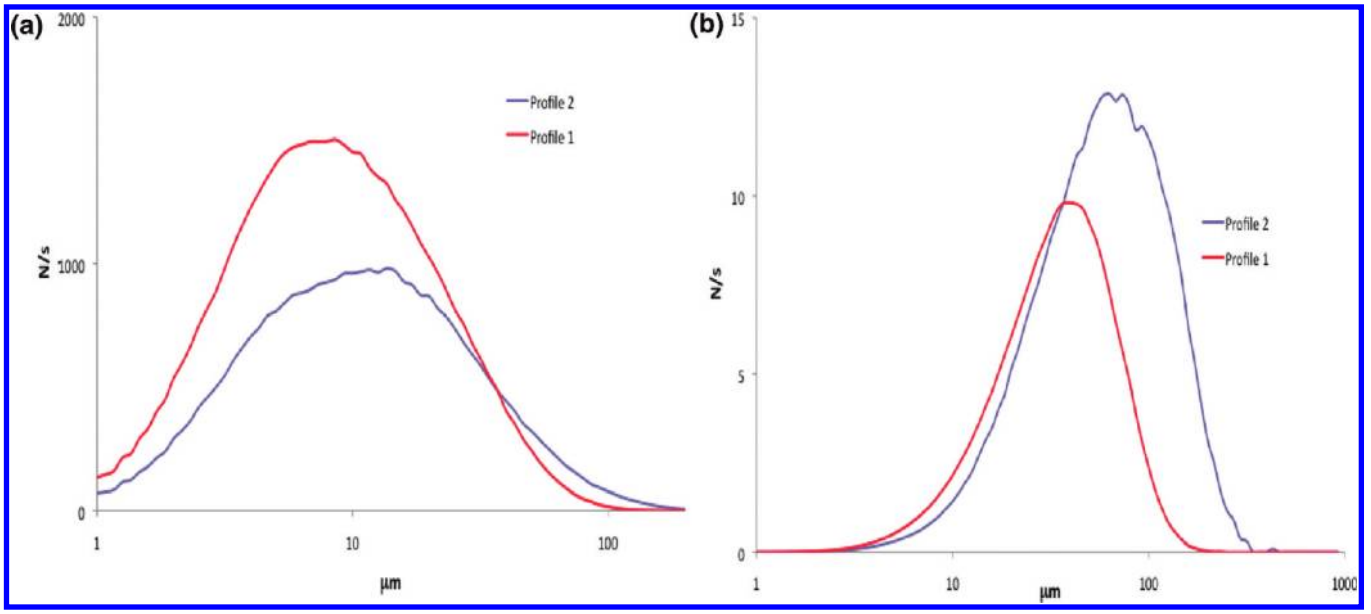

Figure 11. (a) Nonweighted linear chord length distribution. (b) Square-weighted chord length distribution after cooling ramp for profiles 1 and 2. Log distributions are shown, as these lead to a higher resolution.

Figure 8 shows the behavior of some statistical parameters based on the CLD evolution over time. The initial growth of long thin needles is confirmed by the strong increase in the number of large chord lengths counted per second (green curve) during the first 10 min. In parallel, the total needle length (blue curve) rapidly increases, pointing towards a rapid needle growth. The brittleness of these needles is confirmed by the relatively small needle width of about 7.06 μm (nonweighted median between 1 and 30 μm) observed 10 min after nucleation. The crystals obtained easily break up as shown by the successive rapid decrease in the number of large chord lengths counted (green curve) and the decrease in average needle length (red curve).

PVM images (Figure 9) confirm the presence of fine thin needles at the onset of crystallization (Figure 9, left image), and the appearance of shorter, more coarse needles during the remaining part of the crystallization (Figure 9, right image).

Spontaneous crystallization is thus characterized by an initial nucleation of needle-shaped crystals that undergo an important longitudinal growth.

5.3. Seeding. Seeds are added at 53 °C (profiles 2 and 3), 5 °C into the metastable zone, to achieve a controlled initial crystallization. The relative supersaturation at this stage is about 56%. The relatively small amount of seeds (0.2% w/w with respect to the amount of CDP323) provokes an initial crystallization relatively similar to that observed above, [Although overall crystallization characteristics are similar, underlying phenomena are different, as crystallization is induced by respectively primary and secondary nucleation.] characterized by the appearance of a strong initial growth of fine thin needles that easily break up, as well as the appearance of a crystallization exotherm. Dry seeding is performed with agglomerated material [As dry seeding is performed, seeds can indeed be expected to consist of agglomerated crystals.] as can be observed in Figure 10, where one notices a sudden increase in average-sized crystals (blue curve) at t = 1.9 h that show an average width of about 15 μm (purple curve). The successive drop in both average size and average width can be due either to the agglomerates breaking up or to secondary nucleation, which rapidly introduces finer needles, implying the larger seeds are no longer detectable by the probe. Approximately 10 min after seeding, secondary nucleation occurs, as shown by the sudden burst in the number of large (green curve) and small chord lengths counted (brown curve). Initial crystallization is thus comparable to the onset of the spontaneous crystallization observed above with a strong increase in large-sized particles (green curve) that break up during the first 10 min following nucleation.

About 15 min after seeding, secondary nucleation no longer occurs, and one observes a steady increase in the number of average-sized needles (blue curve), as well as a decrease in the number of small chord lengths counted (brown curve). During the isothermal hold, the average needle width furthermore increases (purple curve). These observations are consistent with a so-called 'maturation',[37] characterized by dissolution of smaller crystals in favor of longitudinal and axial growth of the average-sized needles. After a 1-h isothermal hold the average needle width is about 10.7 μm, and the average needle length about 84.9 μm.

The effect of seeding at 53 °C, followed by a 1-h isothermal hold, is best evaluated by comparing the CSD obtained at the end of cooling profiles 1 and 2. Figure 11 shows cooling profile 2 to yield coarser material and fewer fines. The average increased needle width (9.01 μm compared to 7.69 μm) and increased crystal length (87.27 μm compared to 55.76 μm) illustrate the effect of introducing an isothermal hold.

Although the small amount of seeds used provokes an initial crystallization similar to spontaneous crystallization, the introduction of an isothermal hold at seeding temperature influences the final particle size distribution. Control of particle size should therefore be possible by altering seeding temperature, as well as the duration of the isothermal hold.

5.4. Effect of the Cooling Rate. The effect of cooling rate on the crystallization mechanism can be studied, comparing online data from profiles 2 and 3. Both profiles are similar up until the cooling ramp. At this point, profile 2 is characterized by a 20 °C/h cooling rate, while a much slower cooling rate of 1.5 °C/h is used in profile 3. The end point of the 1 h isothermal hold at 53 °C will be taken as a reference point to discuss the effect of the cooling rate.

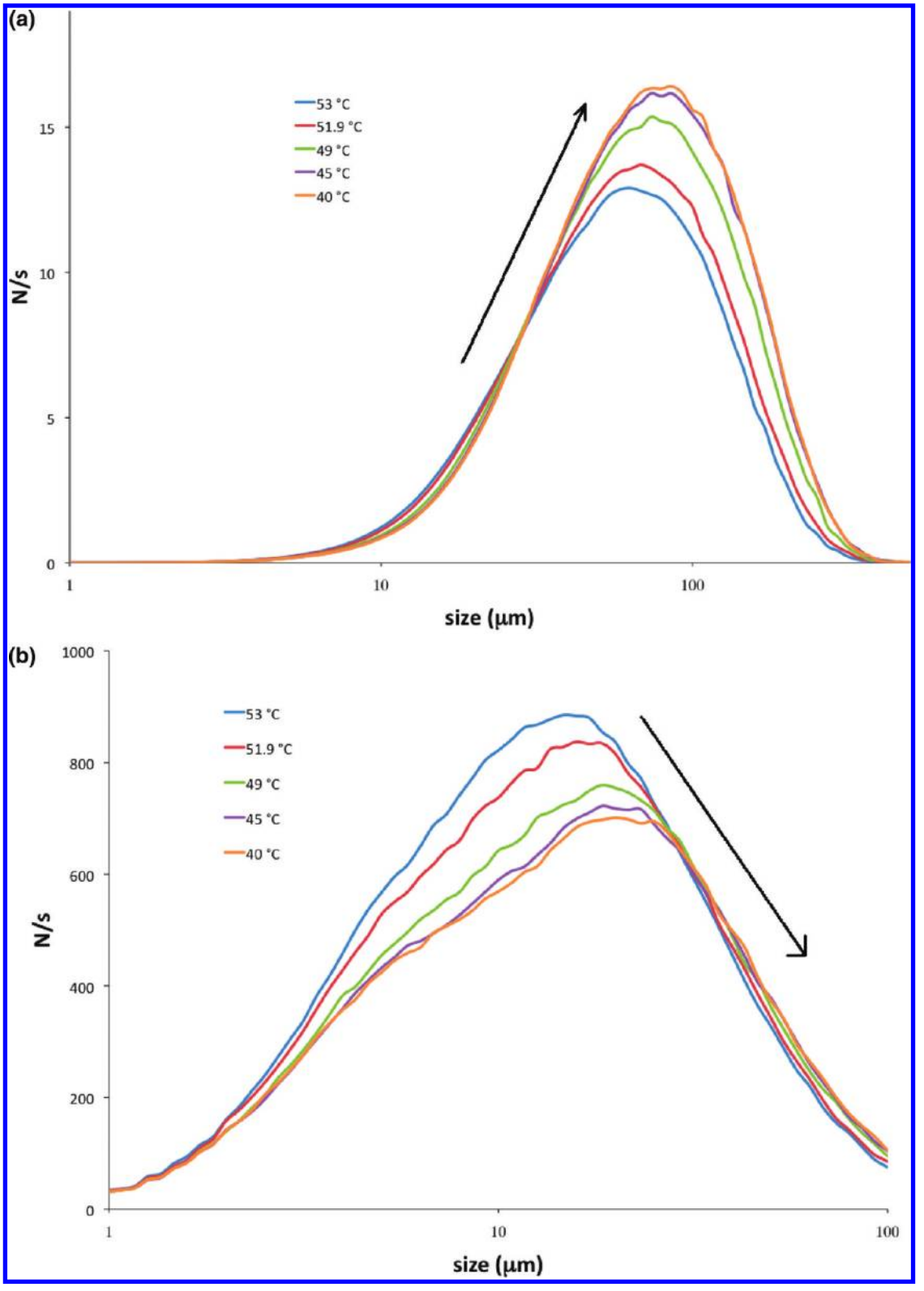

Figure 12. (a) Square-weighted and (b) nonweighted chord length distribution during the 1.5 °C/min cooling ramp.

Two distinct periods are observed for the slow cooling ramp of profile 3 (1.5 °C/h). During the first 8 h of cooling (from 53 °C down to 45 °C), crystal growth predominates as shown by the decrease in unweighted CLDs, combined with their shift towards larger chord lengths and by the increase in square-weighted CLDS, combined with their shift towards larger chord lengths (Figure 12).

Down to 45 °C both the average needle width and the average needle length increase respectively from 10.7 to 11.2 μm, and 84.9 to 98.0 μm, as shown in Figure 13b. The decrease in the

dx.doi.org/10.1021/op100314g |*Org. Process Res. Dev.* 2011, 15, 413–426

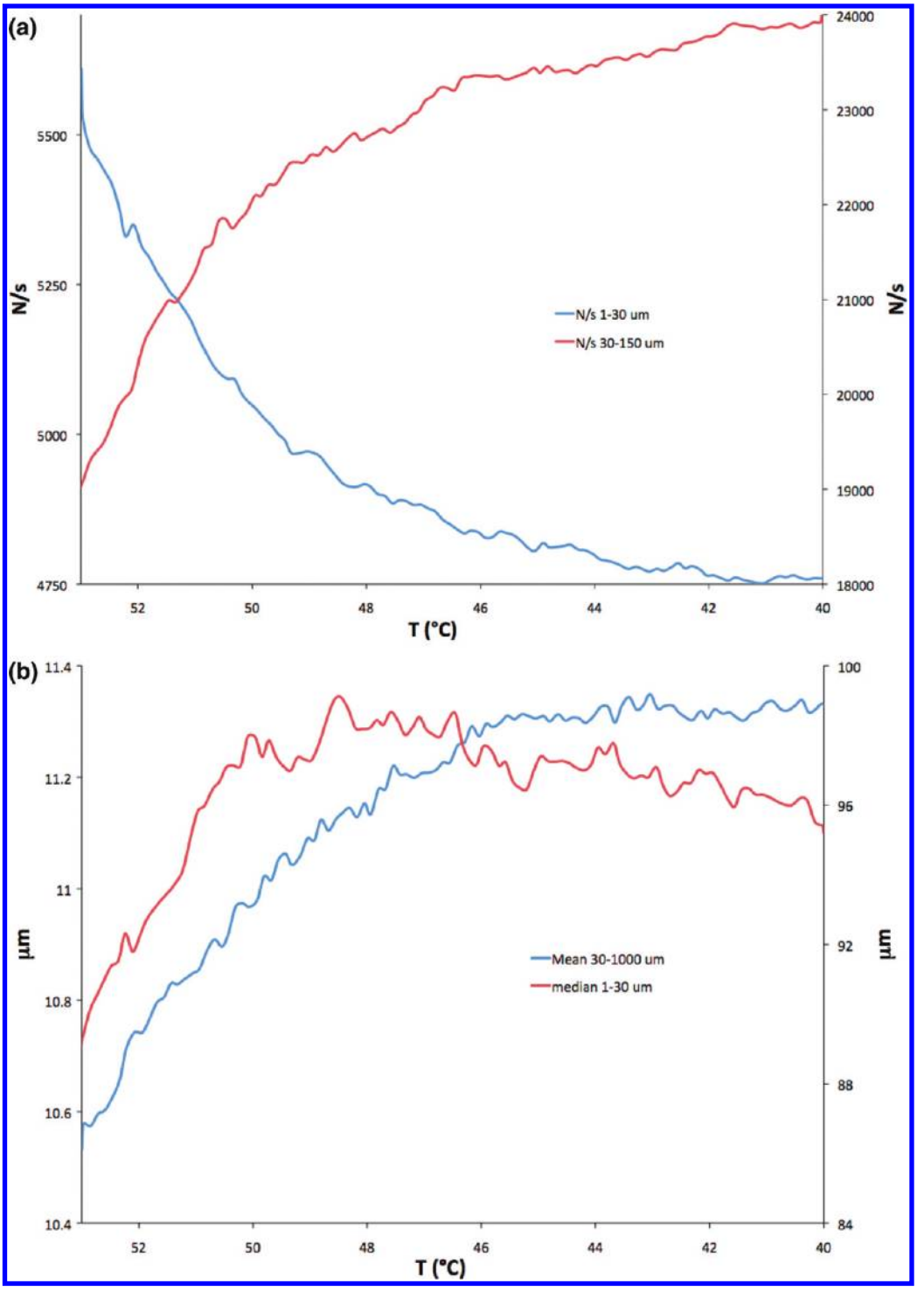

Figure 13. (a) Number of chord lengths counted per second between 1 and 30 μm (blue curve/right axis), 30−150 μm (red curve/left axis). (b) Median chord lengths counted per second between 1 and 30 μm (red curve/left axis), square-weighted mean chord lengths per second between 30 and 1000 μm (blue curve/right axis).

number of small chord lengths counted and the increase in the number of average-sized (Figure 13a) and large-sized chord lengths counted are consistent with crystal growth. Therefore, it seems that for crystal growth down to 46 °C the kinetics are fast enough to desaturate the solution, leading to a low supersaturation level, which in turn reduces secondary nucleation kinetics. At this stage crystal growth rate outweighs the secondary nucleation rate.

From 45 °C onwards, the general behavior of all statistical trends changes. Both average needle width and average needle size decrease respectively from 11.2 to 10.7 μm and 97 to 93 μm (Figure14b). The number of average-sized particles passes through a maximum and then start to decrease, while the opposite behavior is observed for the number of small chord lengths counted. Observations below 30 °C are consistent with secondary

dx.doi.org/10.1021/op100314g |*Org. Process Res. Dev.* 2011, 15, 413–426

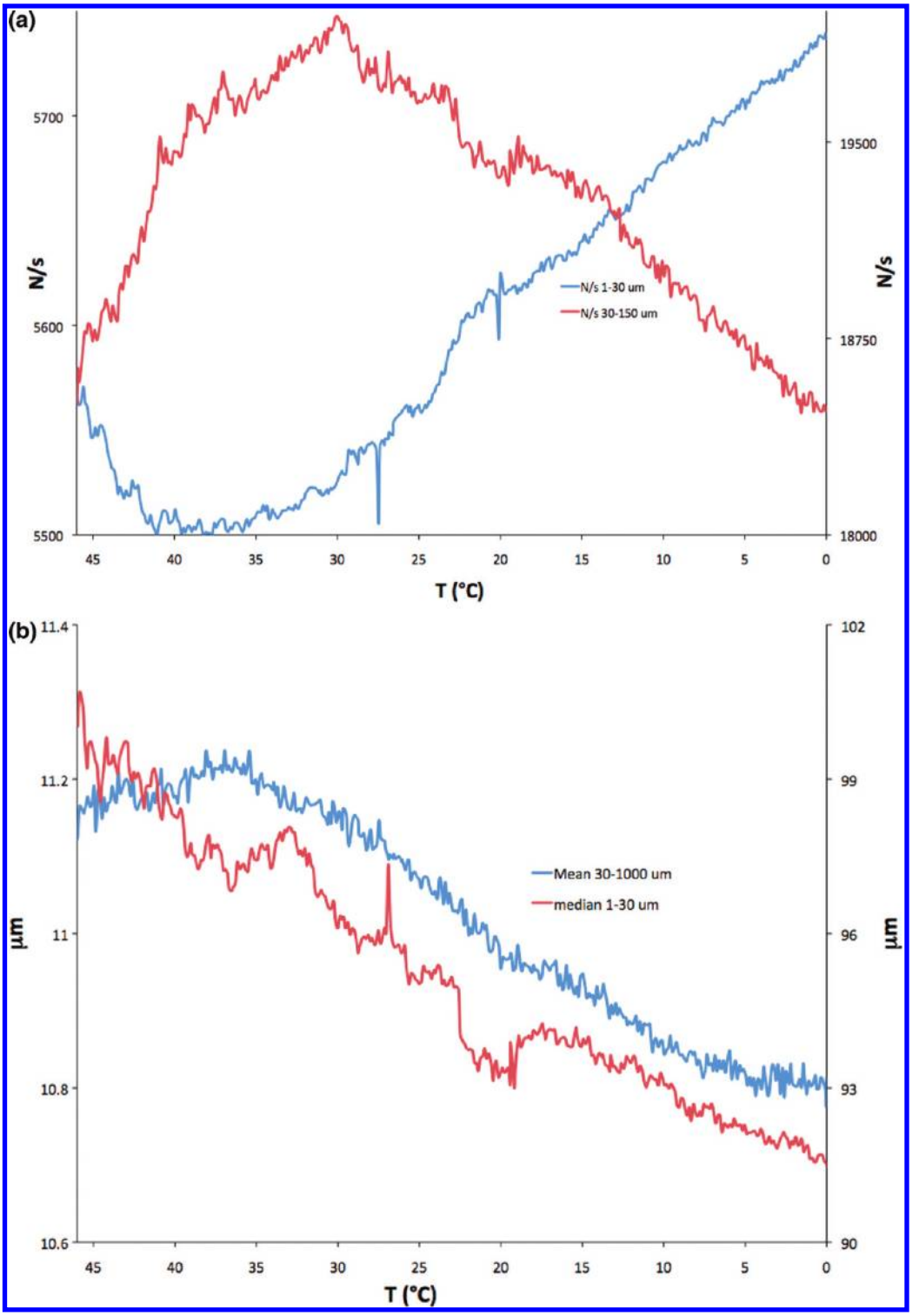

Figure 14. (a) Number of chord lengths counted per second over time between 1 and 30 μm (blue curve/right axis), 30−150 μm (red curve/left axis). (b) Median chord lengths counted per second between 1 and 30 μm (red curve/left axis), square-weighted mean chord lengths per second between 30 and 1000 μm (blue curve/right axis).

nucleation, characterized by the appearance of smaller and finer needle-shaped crystals, hence explaining the decrease in average needle width, as well as size, and the increase in total needle length counted (counts between 1 and 30 μm). The reduction in number of average-sized particles can be explained by a combination of continuous crystal breaking, as well as interference of small particles with the detection probe. Between 45 and 30 °C, a change in dominant mechanism is thus observed, with secondary nucleation rate overthrowing crystal growth rate. Although one could argue that a further reduction of the cooling rate could be applied to promote crystal growth below 30 °C, this would lead to exceptionally long process times and thus, is discarded for this specific crystallization.

dx.doi.org/10.1021/op100314g |*Org. Process Res. Dev.* 2011, 15, 413–426

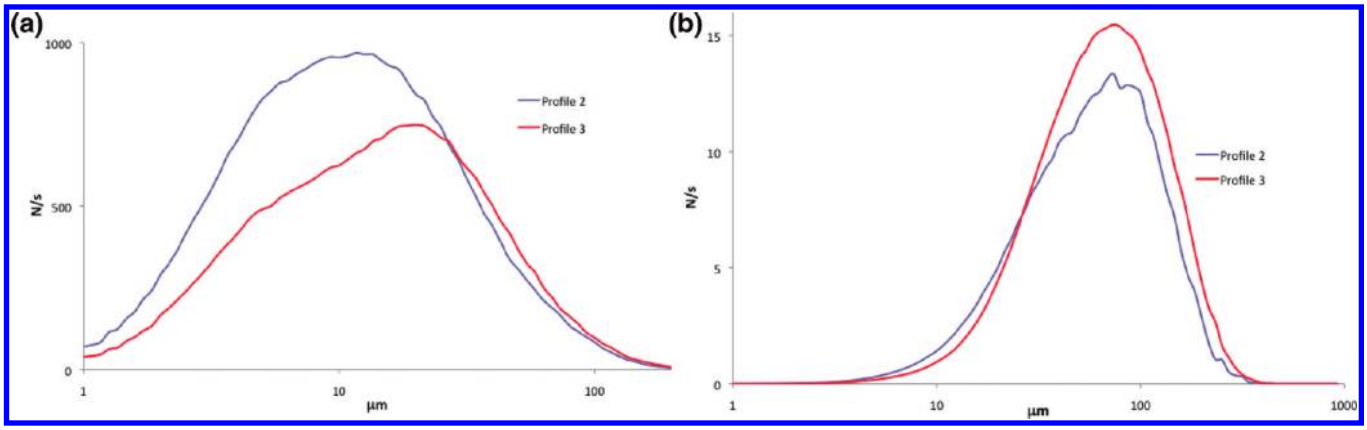

Figure 15. (a) Nonweighted linear chord length distribution. (b) Square-weighted chord length distribution after cooling ramp for profiles 2 and 3. Log distributions are shown, as these lead to a higher resolution.

Using a faster cooling rate of 20 °C/h, a similar behavior is observed, with a first period being dominated by crystal growth, and a second period being dominated by secondary nucleation. Trends vary in a manner similar to that described above, except that secondary nucleation already dominates from 45 °C downwards. From a qualitative point of view, one could thus argue that the crystallization using a more important cooling ramp is characterized by relatively less crystal growth. This is confirmed by comparing the outcome of both cooling profiles, when the temperature of 0 °C is reached. The CSDs shown in Figure 15, confirm that the slower cooling profile leads to coarser material. At the onset of cooling, the average crystal width is about 10.4 μm and the average needle length is about 86 μm. A continuous cooling rate of 1.5 °C/h leads to final material showing an average needle width of about 10.7 and 93 μm in length, whilst finer material is observed applying a 20 °C/h cooling ramp, obtaining crystals of 9.1 μm in average width and 84.6 μm in average length.

5.5. Final Isothermal Hold. Ultimately, the influence of a final isothermal hold at 0 °C was investigated. Similar observations were made for all three experiments. Over 15 h, a slight increase in average needle width of about 0.3 μm is observed, but no changes occur in average needle length. 'Maturation' thus most likely occurs at a very slow rate, and long isothermal holds are not recommended to obtain coarser material in the case of CDP323-2, as the process time would increase substantially for a significant effect to be observed.

6. CONCLUSION

Online in situ follow-up of chord length distributions over time can be used to understand the crystallization mechanism of a batch-cooled crystallization of needle-shaped particles. Due to the particular form of these crystals, specific statistical CLD parameters were defined that allowed estimation of characteristics such as average needle width and average needle length, as well as the study of their variation over time. By combining different characteristics, the dominant mechanism of the crystallization could be distinguished at different stages of the cooling crystallization, and the process could hence be optimized.

In the case of CDP323-2 a fast initial nucleation was observed, even upon seeding, followed by a very rapid longitudinal crystal growth, leading to fine, long and brittle needles that easily break. Seeding could be used to control the timing of the initial nucleation. Introduction of an isothermal hold upon seeding yielded coarser material, due to a so-called 'maturation' period. During the initial stages of cooling, crystal growth kinetics dominate secondary nucleation kinetics. This tendency, however, depends on the temperature and cooling rate. Although a final isothermal hold can influence the final particle size distribution, the time period needed to observe a significant change is estimated to be too long from an economical point of view.

In this contribution, the FBRM probe is shown to be a powerful tool for understanding and optimizing crystallizations. Careful interpretation of the data is required when dealing with nonspherical crystals such as needle-shaped crystals. Statistical analysis of the acquired data leads to meaningful insight into the crystallization mechanism.

■ ASSOCIATED CONTENT

Supporting Information. The solubility curve of CDP323-2 in a 72% v/v EtOH/H_2O mixture. This material is available free of charge via the Internet at http://pubs.acs.org.

■ AUTHOR INFORMATION

Corresponding Author
Tom.leyssens@uclouvain.be

■ ACKNOWLEDGMENT

We thank Drs. J. Hamann and G. Worms for their help in installing a research lab. T.L. also thanks B. O'Sullivan and N. Tyrrell for their help reviewing the article and their useful comments.

■ REFERENCES

(1) Chew, J. W.; Chow, P. S.; Tan, R. B. H. *Cryst. Growth Des.* **2007**, *7*, 1416–1422.
(2) Cote, A.; Zhou, G.; Stanik, M. *Org. Process Res. Dev.* **2009**, *13* 1276–1283.
(3) Mangin, D.; Puel, F.; Veesler, S. *Org. Process Res. Dev* **2010**, *13* 1241–1253.
(4) Yu, Z. Q.; Chew, J. W.; Chow, P. S.; Tan, R. B. H. *Chem. Eng. Res. Des.* **2007**, *85*, 893–905.
(5) Borissova, A.; Khan, S.; Mahmud, T.; Robert, K. J.; Andrews, J.; Dallin, P.; Chen, Z.-P.; Morris, J. *Cryst. Growth Des.* **2009**, *9*, 692–706.

(6) Bakar, A. M. R.; Nagy, Z. K.; Rielly, C. D. *Cryst. Growth Des.* **2010**, *10*, 3892–3900.
(7) Hermanto, M. W.; chow, P. S.; Tan, R. B. H. *Cryst. Growth Des.* **2010**, *10*, 3668–3674.
(8) Gagnière, E.; Mangin, D.; Puel, F.; Bebon, C.; Klein, J.-P.; Monnier, O.; Garcia, E. *Cryst. Growth Des.* **2009**, *9*, 3376–3383.
(9) Boyd, S.; Back, K.; Chadwich, K.; Davey, R. J.; Seaton, C. C. *J. Pharm. Sci.* **2010**, *99*, 3779–3786.
(10) Barret, P.; Smith, B.; Worlitschek, J.; Bracken, V.; O'Sullivan, B.; O'Grady, D. *Org. Process Res. Dev.* **2005**, *9*, 348–355.
(11) Erl, D.; Barnes, S. E.; Cooley, B. E.; Goss, C. A. *Am. Pharm. Rev.* **2009**, *12*, 68–72.
(12) Rodrigues, L. O.; Marques, J. L.; Cardoso, J. P.; Menezes, J. C. *J. Process Anal. Technol.* **2005**, *2*, 12–17.
(13) Birch, M.; Fussell, S.; Higginson, P. D.; McDowall, N.; Marziano, I. *Org. Process Res. Dev.* **2005**, *9*, 360–364.
(14) Yu, L. X.; Lionberger, R. A.; Raw, A. S.; D'Costa, R.; Wu, H.; Hussain, A. S. *Adv. Drug Delivery Rev.* **2004**, *56*, 349–369.
(15) Rohani, S.; Horne, S.; Murthy, K. *Org. Process Res. Dev.* **2005**, *9*, 858–872.
(16) Rohani, S.; Horne, S.; Murthy, K. *Org. Process Res. Dev.* **2005**, *9*, 873–883.
(17) www.FDA.gov
(18) Sparks, R. G.; Dobbs, C. L. *Part. Part. Syst. Charact.* **1993**, *10*, 279.
(19) Tadayyon, A.; Rohani, S. *Part. Part. Syst. Charact.* **1998**, *15*, 127.
(20) Barret, P.; Glennon, B. *Part. Part. Syst. Charact.* **1999**, *16*, 207.
(21) (a) Worlitscheck, J.; Hocker, T.; Mazzotti, M. *Part. Part. Syst. Charact.* **2005**, *16*, 207. (b) Li, M. Z.; Wilkinson, D. *Chem. Eng. Sci.* **2005**, *60*, 4992–5003. (c) Li, M. Z.; Wilkinson, D. *Chem. Eng. Sci.* **2005**, *60*, 3251–3265. (c) Bloemen, H. H. J.; De Kroon, M. G. M. *Part. Sci. Technol.* **2005**, *23*, 377–386. (d) Pons, M. N.; Milferstedt, K.; Morgenroth, E. *Chem. Eng. Sci.* **2006**, *61*, 3962–3973. (e) Vaccaro, A.; Sefcik, J.; Morbidelli, M. *Part. Part. Syst. Charact.* **2007**, *23*, 360–373. (f) Nere, N. K.; Ramkrishna, D.; Parker, B. E.; Bell, W. V.; Mohan, P. *Ind. Eng. Chem. Res.* **2007**, *46*, 3041–3047. (h) Kail, N.; Briesen, H.; Marquardt, W. *Part. Part. Syst. Charact.* **2007**, *24*, 184–192. (i) Kempkes, M.; Eggers, J.; Mazzotti, M. *Chem. Eng. Sci.* **2008**, *63*, 4656–4675. (j) Greaves, D.; Boxall, J.; Kohn, C. A. *Chem. Eng. Sci.* **2008**, *63*, 5410–5419.
(22) Scott, C.; Black, S. *Org. Process Res. Dev.* **2005**, *9*, 890–893.
(23) Devarakonda, S.; Crogysman, J. A.; Myerson, A. S. *J. Cryst. Growth* **1999**, *204*, 525.
(24) Hanaki, K.; Hirasawa, I. *J. Chem. Eng. Jpn.* **2009**, *42*, 386–392.
(25) Loan, M.; Parkinson, G.; Newman, M.; Farrow, J. *J. Cryst. Growth* **2002**, *235*, 482.
(26) Wang, Z.; Wang, J.; Dang, L. *Org. Process Res. Dev.* **2006**, *10* 450–456.
(27) Ma, Y.; Zhu, J.; Chen, K.; Wu, Y.; Chen, A. *J. Cryst. Growth* **2009**, *312*, 109–113.
(28) Kail, N.; Marquardt, W.; Briesen, H. *Ind. Eng. Chem. Res.* **2009**, *48*, 2936–2946.
(29) Worlitschek, J. *Diss. ETH* No. 15189, Zürich, 2003.
(30) Worlitschek, J.; Mazzotti, M. *Cryst. Growth Des.* **2004**, *4*, 891–903.
(31) Ruf, A.; Worlitschek, J.; Mazzotti, M. *Part. Part. Syst. Charact.* **2000**, *17*, 167–179.
(32) Barthe, S.; Rousseau, R. W. *Chem. Eng. Technol.* **2006**, *29* 206–211.
(33) Aamir, E.; Nagy, Z. K.; Rielly, C. D. *Chem. Eng. Sci.* **2010**, *4* 70–74.
(34) Used with permission of Mettler-Toledo Autochem.
(35) Qu, H.; Lanen, K. P.; Louhi-Kultanen, M.; Kilpio, T.; Oinas, P.; Kallas, J. *J. Cryst. Growth* **2005**, *275*, 857–862.
(36) Markande, A.; Nezzal, A.; Fitzpatrick, J. J.; Aerts, L. *Part. Sci. Technol.* **2009**, *27*, 373–388.
(37) Beck, R.; Malthe-Soerenssen, D.; Andreassen, J. P. *Cryst. Res. Technol.* **2010**, *45*, 753–762.
(38) Tyrrell, N. Manuscript in preparation.